SCIENTIFIC REPORTS

OPEN

SUBJECT AREAS:
DRUG REGULATION
CANCER THERAPY

Received
30 April 2014

Accepted
25 July 2014

Published
14 August 2014

Correspondence and requests for materials should be addressed to X.-Z.Z. (xz-zhang@whu.edu.cn)

Multifunctional Enveloped Mesoporous Silica Nanoparticles for Subcellular Co-delivery of Drug and Therapeutic Peptide

Guo-Feng Luo, Wei-Hai Chen, Yun Liu, Qi Lei, Ren-Xi Zhuo & Xian-Zheng Zhang

Key Laboratory of Biomedical Polymers of Ministry of Education & Department of Chemistry, Wuhan University, Wuhan 430072, P. R. China.

A multifunctional enveloped nanodevice based on mesoporous silica nanoparticle (MSN) was delicately designed for subcellular co-delivery of drug and therapeutic peptide to tumor cells. Mesoporous silica MCM-41 nanoparticles were used as the core for loading antineoplastic drug topotecan (TPT). The surface of nanoparticles was decorated with mitochondria-targeted therapeutic agent (Tpep) containing triphenylphosphonium (TPP) and antibiotic peptide $(KLAKLAK)_2$ via disulfide linkage, followed by coating with a charge reversal polyanion poly(ethylene glycol)-blocked-2,3-dimethylmaleic anhydride-modified poly(L-lysine) (PEG-PLL(DMA)) via electrostatic interaction. It was found that the outer shielding layer could be removed at acidic tumor microenvironment due to the degradation of DMA blocks and the cellular uptake was significantly enhanced by the formation of cationic nanoparticles. After endocytosis, due to the cleavage of disulfide bonds in the presence of intracellular glutathione (GSH), pharmacological agents (Tpep and TPT) could be released from the nanoparticles and subsequently induce specific damage of tumor cell mitochondria and nucleus respectively with remarkable synergistic antitumor effect.

During the last decades, intense efforts have been made to construct various drug nanocarriers based on metals[1], metal oxides[2–4], micelles[5], and liposomes[6] for tumor-targeted drug delivery. However, there are many physiological barriers for the nanocarrier reaching the particular target site, including circulating from the blood compartments to the tumor extracellular matrix, sticking to tumor-cell membrane for fast cell internalization, releasing the encapsulated cargo within cells, and targeting to subcellular sites of action in turn. Recently, enveloped nanodevice of programmatically packing the nano-core with different functional groups has been proposed to surmount all these physiological barriers[7,8]. For example, PEGylation is widely used as a stealthy layer for avoiding quick recognition of the carriers by the immune system and thereby extending blood circulation time[9,10]. Moreover, for resisting protein adsorption, negatively charged carriers can be used to block the interaction with cell membrane due to electrostatic repulsion[11]. Nevertheless, positively charged nanoparticles can enter cells easily because of their high affinity to negatively charged cell membrane, although they display rapid clearance from blood circulation[12]. Thus, it is highly desirable to fabricate PEGlated and charge switchable nanoparticles that exhibit good shielding effect against normal cells with a prolonged circulation time, but alter their surface charge at tumor site and become sticky targeting to tumor cells. Positive nanoparticles were reported with the capability to strip stealth layer at acidic environment and re-expose the positively charged surface for improving tumor cell uptake by employing a tumor acidity-sensitive PEGlated anionic polymer[13].

For internalization of nanoparticles by tumor cells, it is essential to liberate therapeutic agents into cytosol or even specific subcellular organelle where most therapeutic agents accumulate and take effect. In contrast to single-agent chemotherapy, combining two or more drugs with synergistic therapeutic effect has been employed for more efficient tumor treatment. As the cellular heart where hereditary material and the transcription machinery reside, the cell nucleus has been demonstrated to be the final targeting destination of various therapeutic agents (*e. g.* genes and antitumor drugs)[14,15]. Thence, traditional combination therapies mainly focused on co-delivery of drug/drug or gene/drug to the cell nucleus[16–21]. Besides, mitochondria, the powerhouse of eukaryotic cells, also play crucial roles in diverse essential cellular functions for cell viability and proliferation as well as programmed

cell death[22]. The specific damage of mitochondria, which would lead to irreversible lethality on cells, renders the possibility of combining two different therapeutic agents targeting to mitochondria and nucleus respectively for combination therapy. To the best of our knowledge, there is no report on co-delivering different therapeutic agents to different subcellular organelles based on a single nanocarrier.

Among different drug delivery systems (DDSs), mesoporous silica nanoparticles (MSNs) are competitive carriers for loading drugs in the pores due to their tunable pore sizes and large pore volumes[23,24]. A variety of pharmaceutical drugs (DOX[25,26], TPT[27], and CPT[28,29]) and fluorescent dyes[30,31] have been encapsulated in MSNs for controlled drug release. In addition, the vast surface functionalization capability[32] allows MSNs to react with diverse agents, including macrocyclic compounds[33–36], polymers[37], dendrimers[38,39], biomacromolecules[40,41], nanoparticles[42–45], and even therapeutic drugs[46]. In this report, a new multifunctional enveloped MSN was designed, *for the first time*, for intracellular co-delivery of antitumor drug and therapeutic peptide to nucleus and mitochondria respectively for synergistic antitumor therapy.

Results

Design of the multifunctional enveloped MSN. As illustrated in Figure 1, an antineoplastic drug topotecan (TPT), as a nuclear enzyme topoisomerase I inhibitor[47], was loaded in the mesopores of MCM-41 type MSN. And the multifunctional enveloped MSN was obtained by programmed packing of mitochondria-targeted therapeutic agent and PEGlated charge conversional shielding layer. For mitochondria-targeted delivery, the lipophilic triphenylphosphonium (TPP) cation as mitochondrial anchor has been demonstrated to effectively deliver payloads into mitochondria[48]. Cationic antibiotic peptide, $(KLAKLAK)_2$, was reported to specially disrupt the mitochondrial membrane and initiate apoptotic death[49]. Conjugating these two domains would give rise to a mitochondria-targeting therapeutic agent TPep, which could traverse the viscous cytosol to the mitochondria sites. Incorporation of PEG-PLL(DMA) on the surface of nanoparticles results in prolonged blood circulation time and good shielding effect against normal cells because of the coexistence of PEG polymers and negatively charged chains. Once arriving at solid tumor site, due to the intrinsic tumor extracellular acidity (pH $\sim$ 6.8)[50], the pH triggered charge conversion occurs (due to the hydrolysis of amide linkages between amines and DMA[51]) accompanied by removing the protecting layer through electrostatic repulsion, in which the surface charge of the enveloped MSN changes to positive. Accordingly, this promotes its internalization by tumor cells with superior efficacy in delivering therapeutic agents. In the presence of intracellular glutathione (GSH), TPep could be released from the nanoparticles by cleavage of the disulfide bonds. Thereafter, the lipophilic TPP would targetedly transport $(KLAKLAK)_2$ to the mitochondria, inducing the dysfunction of mitochondria and killing tumor cells. Meanwhile, TPT loaded in the inner core can be released in cells, leading to much enhanced therapeutic effect together with TPep.

Preparation and characterization of the multifunctional enveloped MSN. The modular therapeutic peptide sequence K-$(KLAKLAK)_2$-C was synthesized by Fmoc-based solid-phase synthesis manually[52] and TPP was conjugated to the last N-terminal group of the peptide. The molecular weight was analyzed by the MALDI-TOF-MS and the purity was analyzed by HPLC (Table S1).

The outer protecting layer PEG-PLL(DMA) was obtained by the ring-opening polymerization of ε-benzyloxycarbonyl-$_L$-lysine N-carboxyanhydriade (Z-Lys-NCA) initiated by the terminal amino group of PEG (Mw 2000), followed by deprotection of the carbobenzyloxy groups and modification with 2,3-dimethylmaleic anhydride

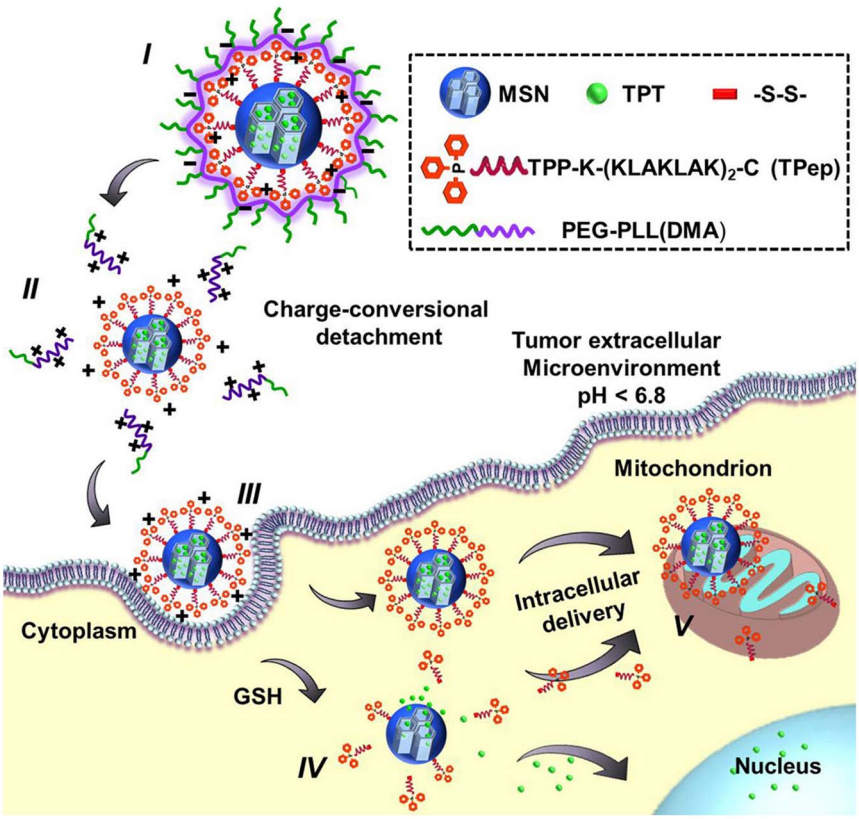

Figure 1 | Schematic design of the delivery process: (I) multifunctional enveloped nanocarrier under physiological condition, (II) charge-conversional detachment of PEGlated corona in acidic tumor microenvironment, (III) adsorption-interaction between positively charged nanoparticles and cell membrane, (IV) intracellular glutathione-triggered TPep & TPT release, (V) specific binding and disrupting of mitochondria.

DMA (Supplementary Figure S1). The ^{1}H nuclear magnetic resonance (^{1}H NMR) of PEG-PLL(Z) was revealed in Figure S2, which proved the successful synthesis of PEG-PLL(Z). The molecular weight of PEG-PLL was calculated as 8.14×10^3 g/mol (Mn) and the degree of polymerization was determined to be 48, which was confirmed by ^{1}H NMR (Supplementary Figure S3A). Gel permeation chromatographic (GPC) measurement of PEG-PLL exhibited a single sharp peak at Mw of 6.90×10^3 g/mol (PDI: 1.3). The ^{1}H NMR spectrum of PEG-PLL(DMA) (Figure S3B) confirmed that ~81% of the amino groups in PLL block were converted to the amide bonds.

MCM-41 type of MSN was prepared by a base-catalyzed surfactant-directed self-assembly procedure. Scanning electron microcopy (SEM) (Figure 2A) and transmission electron microscopy (TEM) (Figure 2B) images showed an average diameter of about 120 nm with a monodisperse distribution of the nanoparticles. And the pore diameter was calculated as ~3 nm (Figure 2B). Dynamic light scattering (DLS) data (Figure 2C) presented a relatively larger diameter due to the hydrated layer surrounding the particles with a narrow particle size distribution. The consecutive modification processes (Supplementary Figure S4) were monitored by zeta potential measurements. As summarized in Figure 2D, the zeta potential of original MSN was −30.7 mV. After surface functionalization by mercapto groups, MSN-SH was obtained with a slightly increased but still negatively charged surface (−23.2 mV). The mercapto groups were then activated by treating with 2,2′-dipyridyl disulfide. Subsequently, TPep containing a free cysteine residue was introduced by disulfide exchange reaction, gaving rise to positively charged nanoparticle (35.2 mV) which was very important for coating polyanion layer on the external surface. Finally, the tumor acidity-responsive anionic PEG-PLL(DMA) was anchored to the surface of positively charged MSN-TPep nanoparticle by electrostatic interaction for preparing negatively charged MSN-TPep/PEG-PLL(DMA) nanoparticle (−12.4 mV). Nitrogen adsorption-desorption measurements (Figure 2E) revealed that the BET surface area, BJH pore volume and pore diameter decreased progressively after each functionalization step. Moreover, by thermogravimetric analysis (TGA) (Figure 2F), an increased weight loss was obtained: 13.3% for MSN, 20.7% for MSN-SH, 27.5% for MSN-TPep, and 33.2% for MSN-TPep/PEG-PLL(DMA) respectively, further confirming the successful modification.

The multifunctional enveloped MSN-TPep/PEG-PLL(DMA) nanoparticle was expected to exhibit a negative-to-positive charge conversion property in acidic condition due to the degradation of DMA blocks. As shown in Figure 2G, the zeta potential of MSN-TPep/PEG-PLL(DMA) increased obviously from negative (−13.7 mV) to positive (5.4 mV) within 90 min at pH 6.8 and finally reached to about 24 mV after 5 h. In contrast, at pH 7.4, the zeta potential remained at around −12 mV within 5 h. The hydrolysis of amides linkages between amines and DMA made the outer corona detachable under tumor acidic environment. And subsequently, the cell-interactive cationic nanoparticles were obtained, which will be fascinating for tumor targeted delivery.

Evaluation of the tumor-acidity-triggered targeting of the multifunctional enveloped MSN. To evaluate the tumor extracellular acidity triggered targeting, confocal laser scanning microscopy (CLSM) was utilized to observe the cellular uptake. Noted here, the TPep agents were tagged with Rh B (defined as TPep(Rh B)) for observing their intracellular distribution. The reticulum structures of mitochondria were observed as green fluorescence after stained with Mito Tracker Green FM. Free TPep(Rh B) and MSN-TPep(Rh B)/PEG-PLL(DMA) were co-incubated with KB cells (human mouth epidermal carcinoma cells) at different pHs for 4 h. As shown in Figure 3A and Figure 3B, nearly no red fluorescence was observed at both pH 7.4 and 6.8, indicating that free TPep(Rh B) was unable to penetrate into cells. However, there was a appreciable difference in cellular uptake of MSN-TPep(Rh B)/PEG-PLL(DMA) at different pHs. As shown in Figure 3C, there was weak red fluorescence in cells at pH 7.4, indicating the inefficient uptake of particles by cells, mainly attributed to the shielding effect of the unrevoked PEGlated layer. Comparatively, as shown in Figure 2G, the hydrolysis of the amide bonds at pH 6.8 resulted in the charge reversal of PEG-PLL(DMA) from negative to positive, leading to electrostatically removing of the

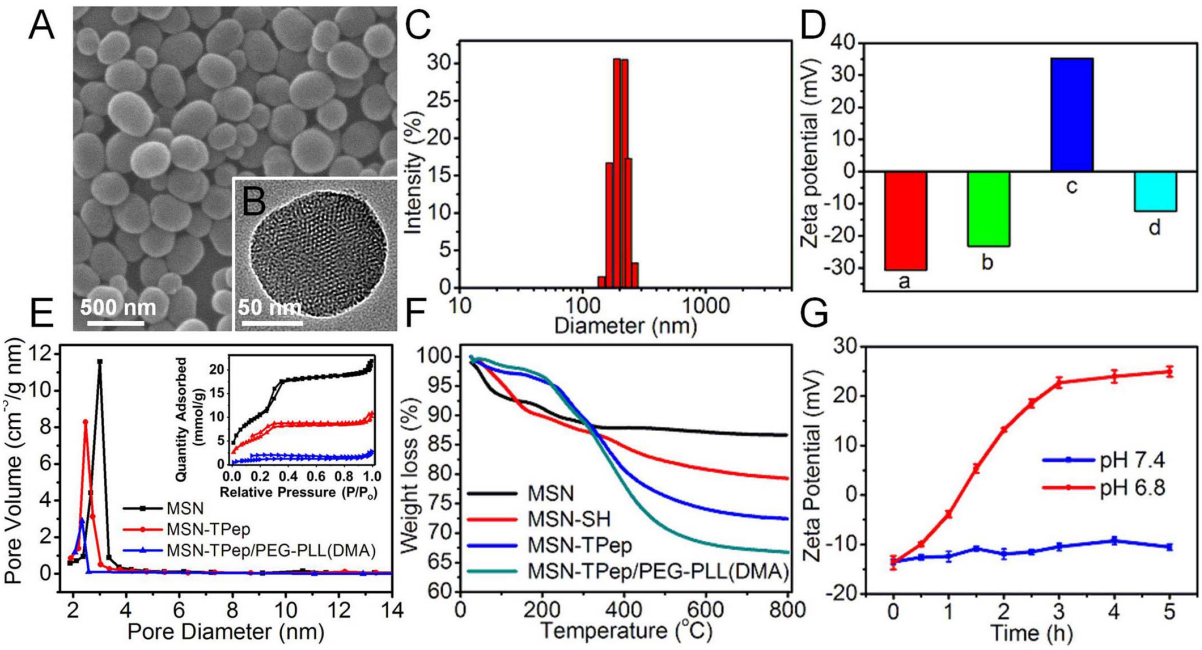

Figure 2 | Characterization of the multifunctional enveloped MSN. (A) SEM image of MSN. (B) TEM image of MSN. (C) DLS analysis of MSN. (D) Zeta-potentials of (a) MSN, (b) MSN-SH, (c) MSN-TPep, (d) MSN-TPep/PEG-PLL(DMA). (E) Pore size distribution of MSN, MSN-SH, MSN-TPep, MSN-TPep/PEG-PLL(DMA). Inset: Nitrogen adsorption−desorption isotherms. (F) TGA curves of different nanoparticles. (G) Zeta-potential changes of MSN-TPep/PEG-PLL(DMA) as a function of incubation time at pH 7.4 and 6.8.

PEGlated protecting layer. After removal of the PEGlated protecting layer, the positively charged MSN-TPep(Rh B) nanoparticles were favorable for subsequent cellular uptake. And thus the red fluorescence in cells at pH 6.8 dramatically enhanced (Figure $3D_2$). Moreover, the merged picture of Figure $3D_3$ showed strong yellow fluorescence, indicating the co-localization of red TPep(Rh B) and green mitochondria. As further revealed in Figure 3E, which represents the relative fluorescence intensity corresponding to the white line in Figure $3D_3$, the fluorescence from red Rh B and green Mito Tracker matched well. However, no significant overlapping areas were observed in the merged image of cells treated with non-TPP-conjugated particles (Supplementary Figure S5). This difference was ascribed to the specific mitochondria targeting ability of TPP, which was consistent with the literature report that TPP facilitates the entrance of small molecules or nanosystems into mitochondria efficiently by its electrophoretic force and lipophilicity[53,54]. The ability of mitochondrial targeting provided a good platform for mitochondria-targeted drug delivery.

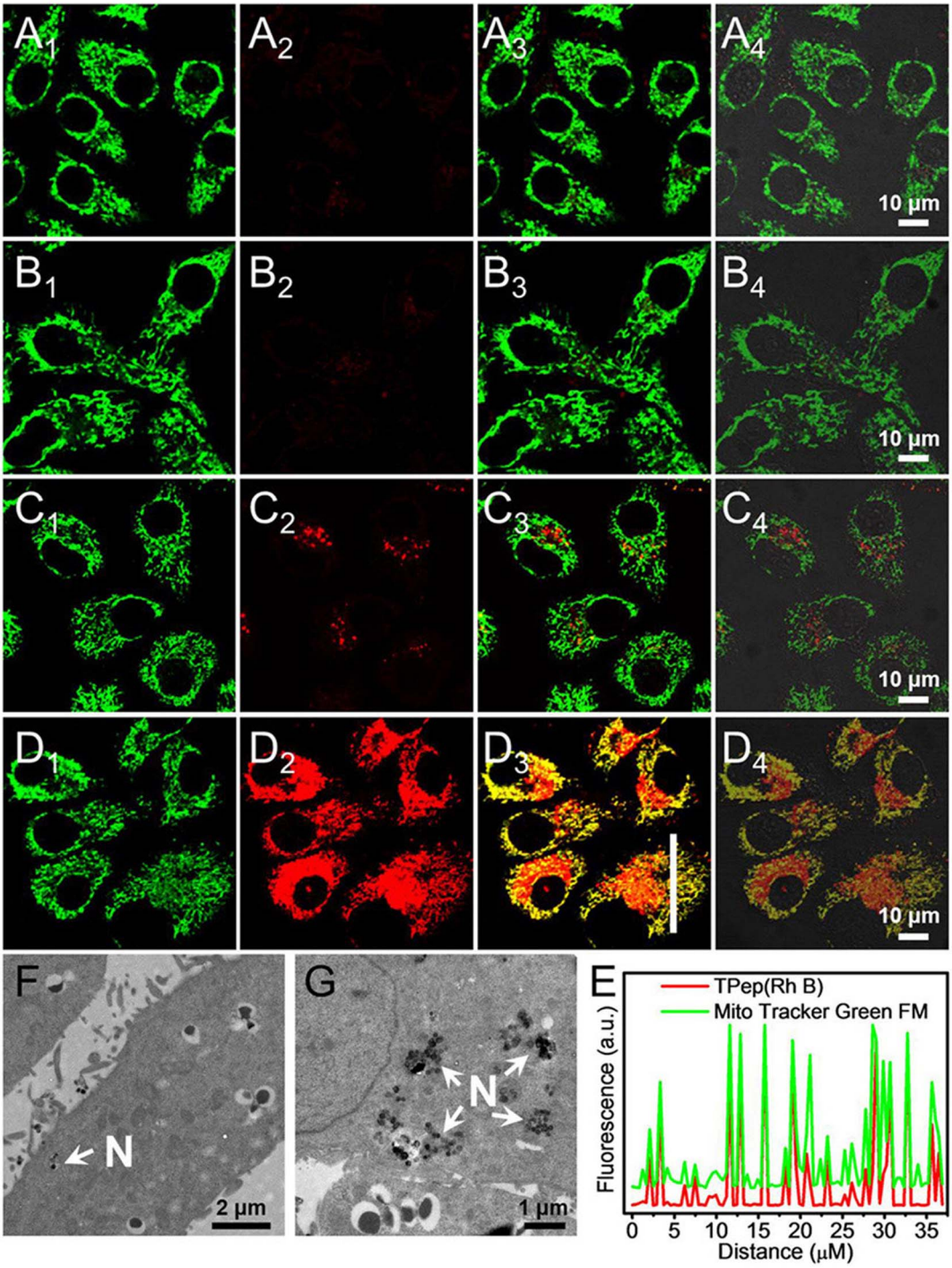

Figure 3 | CLSM images of KB cells treated with free TPep(Rh B) (A), (B) and MSN-TPep(Rh B)/PEG-PLL(DMA) (C), (D) at pH 7.4 (A), (C) and 6.8 (B), (D) for 4 h. (A_1, B_1, C_1 and D_1) green fluorescence images; (A_2, B_2, C_2 and D_2) red fluorescence images; (A_3, B_3, C_3 and D_3) confocal fluorescence images; (A_4, B_4, C_4 and D_4) overlay of confocal fluorescence and bright field images. (E) Fluorescence signals corresponding to the white line in D_3. (F) TEM images of KB cells treated with MSN-TPep/PEG-PLL(DMA) at pH 7.4 and (G) at pH 6.8. The white arrows indicate the nanoparticles (N).

The cell uptake of MSN-TPep/PEG-PLL(DMA) at different pHs were also confirmed by Bio-TEM observation. A similar phenomenon was observed. Very little particles existed in cells at pH 7.4 (Figure 3F), while an increased amount of nanoparticles were observed in cells at pH 6.8 (Figure 3G), further suggesting a pH-dependent cell uptake of the enveloped MSN-TPep/PEG-PLL(DMA) nanoparticles.

Moreover, flow cytometry analysis was carried out to quantitatively evaluate the amount of cellular uptake of free TPep(Rh B) and MSN-TPep(Rh B)/PEG-PLL(DMA) (Supplementary Figure S6). Free TPep(Rh B) gave a minimum cell uptake at both pHs (Supplementary Figure S6A and S6B). For cells treated with nanoparticles, there was a 3.8-fold increase of the mean fluorescence intensity (MFI) in cells incubated at pH 6.8 compared with that at pH 7.4. Evidently, the enveloped MSN-TPep(Rh B)/PEG-PLL(DMA) exhibited the ability of tumor-acidity-triggered targeting and efficient delivering of TPep to tumor cell mitochondria.

Evaluation of the specific mitochondria damage by JC-1 assay and Bio-TEM observation. As we know, the disulfide bonds embedded in the nanoplatform are able to respond to intracellular GSH for a triggered release behavior[55]. For TPep(Rh B) release study, the loading content of TPep(Rh B) in MSN-TPep(Rh B)/PEG-PLL(DMA) was ~9.6% by measuring the fluorescence emission of Rh B. As shown in Figure S7, for nanoparticles incubated in the absence of GSH or in the presence of GSH at pH 7.4, the TPep(Rh B) release from MSN-TPep(Rh B)/PEG-PLL(DMA) was very slow due to the blocking effect of the outer shielding layer and the inefficient breakage of the disulfide bonds. However, after treating with 10 mM GSH at pH 6.8 for 24 h, maximum release amount (65% of TPep(Rh B)) was detected. This result suggested that enveloped nanocarrier offered a controlled release system for intracellular GSH response, which would not release the therapeutic peptide before entering tumor cells.

To investigate the mitochondrial damage/disruption by released TPep, MSN-TPep/PEG-PLL(DMA) were incubated with KB cells with mitochondrial fluorescence probe JC-1 analysis. As we know, the mitochondrial transmembrane potential ($\Delta\Psi_m$) is an important indicator of mitochondrial functions. The drop of mitochondrial membrane potential is usually considered as the hallmark for mitochondrial dysfunction. Thus, the change in $\Delta\Psi_m$ has been used to evaluate mitochondrial death[56]. This change can be indicated by JC-1 probe for distinguishing damaged mitochondria from normal ones. As shown in Figure 4, for cells co-incubated with nanoparticles at pH 7.4 for different time (Figure 4B and 4C), the green and red fluorescence did not show significant difference to that of untreated cells (control group, Figure 4A). JC-1 mainly accumulated in mitochondria to generate the red J-aggregates (J-aggre) along with slight green fluorescent monomeric form remained in the cytoplasm. Whilst, in the case of pH 6.8 (Figure 4D for 12 h and Figure 4E for 36 h, respectively), the collapse of $\Delta\Psi_m$ was observed by the gradually increased J-monomer green fluorescence in cytoplasm and simultaneously the decrease of J-aggre red fluorescence (normal mitochondria) with the prolonged incubation time, which demonstrated the serious damage of mitochondria.

To visualize the mitochondrial damage directly, morphological evidence was further provided by Bio-TEM observation. For KB cells without treating with nanoparticles, the mitochondria maintained the morphology of normal orthodox conformation in healthy cells. (Figure 5A). However, after treating with MSN-TPep/PEG-PLL(DMA) particles (Figure 5B, C, D, E), unusual morphologies and serious damage of mitochondria were observed. As shown in Figure 5B and 5C, most of the mitochondria showed irregular swelling (pentacle) and severe vacuolization (doji star). Moreover, some of the mitochondrial membrane was broken (yellow doji star), which was considered for leaking out of the mitochondrial matrix. On the other hand, a number of black dots were found at the areas of mitochondria, which were identified to be the nanoparticles according to the shape and size (Figure 5D and 5E). This may be ascribed to the targeting ability of TPP. Furthermore, a significant silicon signal from energy-dispersive X-ray (EDX) (Figure 5F) was detected, also suggesting the the localization of nanoparticles in mitochondria.

Investigation of the drug loading capability and antitumor efficiency of the multifunctional enveloped MSN. To address the co-delivery capability of multifunctional MSNs, an antineoplastic drug topotecan (TPT), was further loaded in the pores of the enveloped MSN. CLSM observations revealed a similar tumor-acidity-triggered cellular uptake for TPT loaded nanoparticles (TPT@MSN-TPep(Rh B)/PEG-PLL(DMA)). As shown in Figure S8, the red fluorescence (TPep(Rh B)) and green fluorescence (TPT) intensity in KB cells at pH 6.8 were dramatically enhanced, while both the fluorescence were negligible in cells at pH 7.4. Furthermore, according to fluorescence measurement, about 2.65% TPT was loaded into the mesopores of the nanoparticles. While, accelerated TPT release was monitored with the treatment of GSH at pH 6.8 (Figure 6), suggesting that the pores became opened after removal of the outer corona under acidic condition and discarding the TPep moieties with the presence of GSH.

Furthermore, *in vitro* MTT assays were applied to explore the antitumor efficiency of the multifunctional enveloped nanoparticles. A scrambled peptide, $K_4L_2ALA_2K_2LAKC$, was used as a negative control[48]. TPP was also conjugated to the control peptide, designated as TPep*. As shown in Figure 7A, the cell viability of KB cells remained above 90% when they were treated with free TPep and TPep* up to a concentration of 25 mg/L at different pHs. For the cells treated with MSN-TPep*/PEG-PLL(DMA) (Figure 7B), similar low cytotoxicity were observed. The cell viability remained as high as 85% even at a concentration of 100 mg/L, suggesting that these nanoparticles had inappreciable toxic effect on cells. In addition, the cytotoxic effect of MSN-TPep/PEG-PLL(DMA) was tested. As shown in Figure 7C, obvious cell cytotoxicity was not detected for cells treated with nanoparticles at pH 7.4. While at pH 6.8, MSN-TPep/PEG-PLL(DMA) exhibited a significant cytotoxicity to tumor cells after co-incubation for 48 h. Only 29.8% of cells remained survival with the concentration up to 100 mg/L (corresponding to ~9.6 mg/L of TPep). The accelerated TPep release from the nanoparticles triggered by intracellular GSH should be responsible for the increased cytotoxicity of the MSN-TPep/PEG-PLL(DMA).

To testify the advantage of co-delivery of a drug and therapeutic peptide, the cell viability of KB cells treated with TPT@MSN-TPep*/PEG-PLL(DMA) and TPT@MSN-TPep/PEG-PLL(DMA) were also evaluated. Due to the presence of outer protecting layer (PEG-PLL(DMA)) at pH 7.4, the nanoparticles were blocked to enter into tumor cells. Thus, both TPT@MSN-TPep*/PEG-PLL(DMA) and TPT@MSN-TPep/PEG-PLL(DMA) nanoparticles did not exhibit significant cytotoxicity to cells at pH 7.4 (Figure 7D). However, at the tumor acidic microenvironment (pH 6.8), the outer protecting layer was removed and improved cell lethality was observed for cells treated with TPT@MSN-TPep*/PEG-PLL(DMA). And the cell viability was lower than the corresponding non TPT loaded MSN (Figure 7B) at the same concentration. Moreover, the viability of KB cells incubated with free TPT is almost the same at pH 6.8 or 7.4 (Figure S9), indicating that pH value has no influence on the cell activity under treatment of free drugs. Thus, the desired therapy to tumor cells with our enveloped MSNs was due to the TPT release upon the trigger of intracellular GSH. In comparison with the above results, a more significant antitumor activity was found in TPT@MSN-TPep/PEG-PLL(DMA) treated cells (11% of cells remained survival at pH 6.8 after incubation for 48 h), which was attributed to the additional inhibition of TPep. Thus, TPep and TPT co-

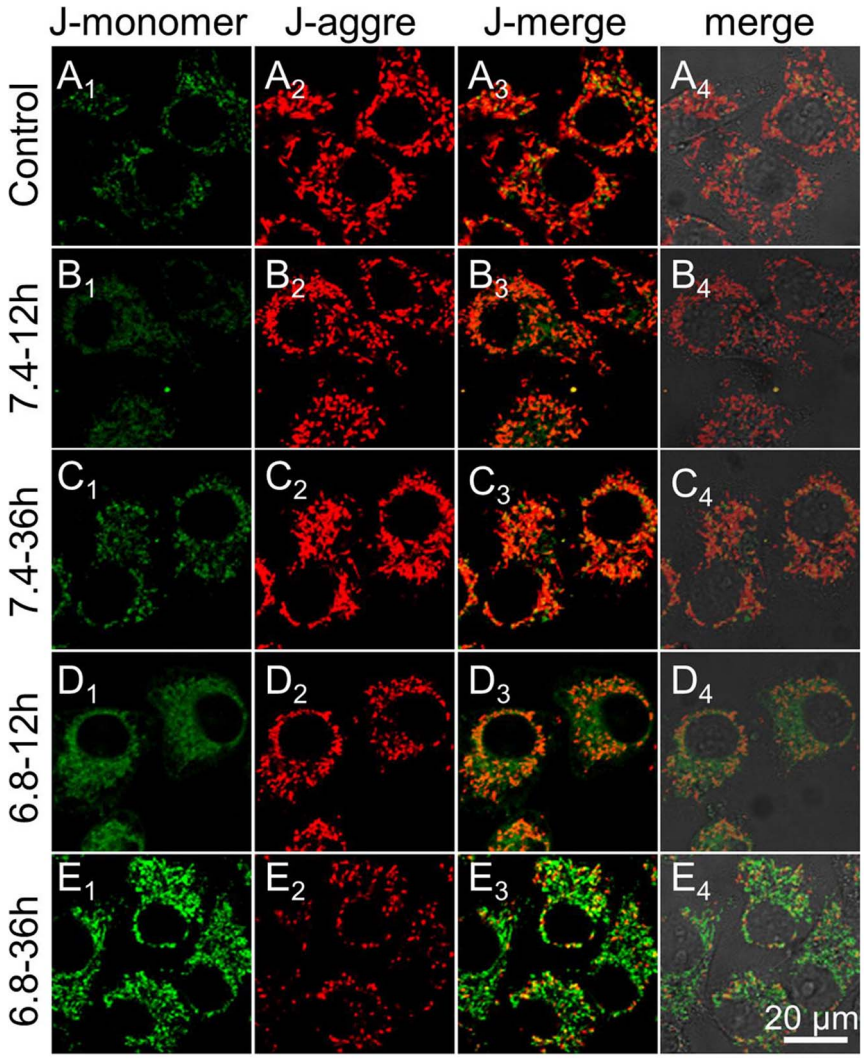

Figure 4 | CLSM images with JC-1 assay of KB cells (A) without treatment; (B) and (C) with MSN-TPep/PEG-PLL(DMA) treatment at pH 7.4 for 12 h and 36 h, respectively; (D) and (E) with MSN-TPep/PEG-PLL(DMA) treatment at pH 6.8 for 12 h and 36 h, respectively.

delivered by the enveloped MSN could suppress cancerous cell growth more efficiently with the synergistic effect.

Discussion

In this study, a multifunctional enveloped nano-carrier (TPT@MSN-TPep/PEG-PLL(DMA)) was constructed for intracellular co-delivery of two different therapeutic agents for synergistic therapy. Well dispersed mesoporous silica nanoparticles with particle size of ~120 nm and pore diameter of ~3 nm were successfully prepared, which presented the capability for encapsulating antitumor drug TPT in their mesopores. Following the programmed package of therapeutic peptide (TPep) and PEG-PLL(DMA) on the surface of nanoparticles, we also demonstrated that such enveloped MSN provided a strategy of targeted delivering pharmaceutical agents into tumor cells. Amides with β-carboxylic acid groups were highly sensitive to pH alteration. Thus, the introduction of DMA moiety into PEG-PLL chains made the polymer become charge reversible. At normal physiological pH, the amide bonds in PEG-PLL(DMA) were stable. But at tumor acidic environment, the amide bonds can degrade to expose positively charged amines, resulting in the removal of stealth layer from the sheddable nanoparticles due to electrostatic repulsion. Scilicet, the surface charge of nanocarriers was sensitive to environmental pH. The enveloped nanoparticles maintained their stealth character during circulation in blood. Once arriving at tumor site, the surface charge of nanoparticles became reversed and the nanoparticles transformed into a more cell-interactive form to display enhanced interaction with tumor cells due to electrostatic attraction. Compared to the cells incubated with enveloped nanoparticles at pH 7.4, much more nanoparticles could be internalized by cells at pH 6.8, indicating superior efficacy in delivering therapeutic agents of our nanocarriers.

The therapeutic peptide TPep was composed of three parts: 1) a free cysteine residue which was favorable for anchoring onto mercapto group functionalized MSN (MSN-SH) via disulfide bonds for GSH triggered release; 2) a lipophilic TPP moiety for mitochondria targeting; and 3) a cationic antibiotic peptide $(KLAKLAK)_2$. It is well known that the GSH concentration in bloodstream (2 μM in plasma) and within cells (1–10 mM) is substantially different[57], which provided the potential to develope GSH-sensitive nanodevices for selective release in living cells. Our results displayed that TPep and TPT could be successfully released from the nanoparticles due to the breakage of the disulfide bonds when the concentration of GSH is 10 mM. However, even after 2 weeks' incubation of the nanoparticles in the absence of GSH, negligible TPep(Rh B) or TPT was released from nanocarriers (Figure S10), indicating the good stability of the enveloped MSNs for storing drugs.

According to CLSM and bio-TEM images, we detected serious mitochondrial damage when KB cells were treated with the

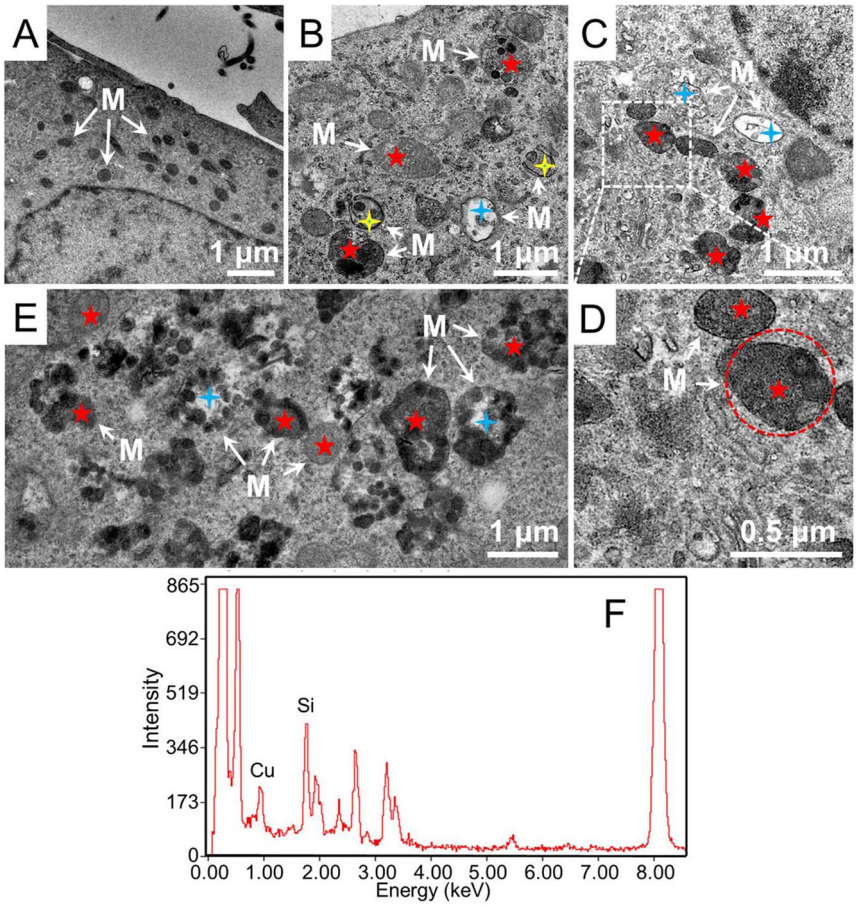

Figure 5 | TEM images of (A) untreated KB cells (control group), (B) (C) and (E) KB cells treated with MSN-TPep/PEG-PLL(DMA) (50 mg/L) for 36 h at pH 6.8, and (D) enlarged rectangular area in C. (F) Energy-dispersive X-ray analysis of the selected area in D (red circle). The white arrows indicate the morphologies of mitochondria (M).

enveloped MSNs at pH 6.8, including an obvious decline in membrane potential ($\Delta\Psi_m$) and the apperance of unusaual mitochondrial morphology (cristae shrunk, swollen, vacuolization, and even broken). These data demonstrated that the released Tpep have the ablity to induce cell apoptosis via the intrinsic mitochondria-dependent apoptosis pathway. In the cytotoxicity study, nanoparticles without therapeutic agents displayed negligible cytotoxicity, indicating good biocompatibility of the mesoporous silica nanoparticles. However, introduction of TPep into the nanocarriers gave rise to a significant reduction in cell viability. In addition, loading of TPT in the mesopores could further enhance the antitumor efficacy remarkably to realize the combined therapy with the synergistic effect.

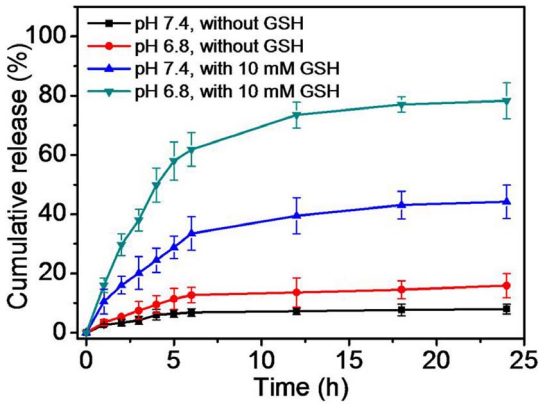

Figure 6 | **The control-release profiles of TPT at different conditions.**

It is worth noting that the multi-chemical modification could tailor the surface property of MSNs, which in turn influence their biological activities including biodegradability, biocompatibility, and bio-elimination of mesoporous silica. Although various bio-safety evaluations have provided a series of evidences that MSNs are biocompatible *in vivo* within desirable dose, and they can be degraded and expelled from the body via urine and feces[58–61], there remain many challenges that need to be overcome since the *in vivo* therapeutic use requires more strict performance modulation to satisfy the complicated physiological environment so as to avoid unwanted bioperformances of MSNs.

To conclude, a multifunctional enveloped nano-carrier was constructed by programmed packing mitochondria-targeted therapeutic agent and charge-conversional shielding layer onto MSNs. Such multifunctional enveloped MSN exhibited ability of tumor acidic-triggered switching in surface charge. *In vitro* results demonstrated a significant enhancement of tumor cellular uptake, excellent mitochondria damage ability, and improved antitumor efficiency of the multifunctional enveloped MSN. Moreover, antineoplastic drug TPT co-delivered by the carrier could further inhibit the growth of tumor cells with remarkable synergistic effect. The multifunctional enveloped MSN demonstrated here open a window for subcellular co-delivery of various therapeutic agents and will find great potential for tumor therapy.

Methods

Materials. Tetraethylorthosilicatem (TEOS), N-cetyltrimethylammonium bromide (CTAB), ninhydrin, hydrazine hydrate, Rhodamine B, and trifluoroacetic acid (TFA) were purchased from Shanghai Reagent Chemical Co. Triphosgene was obtained

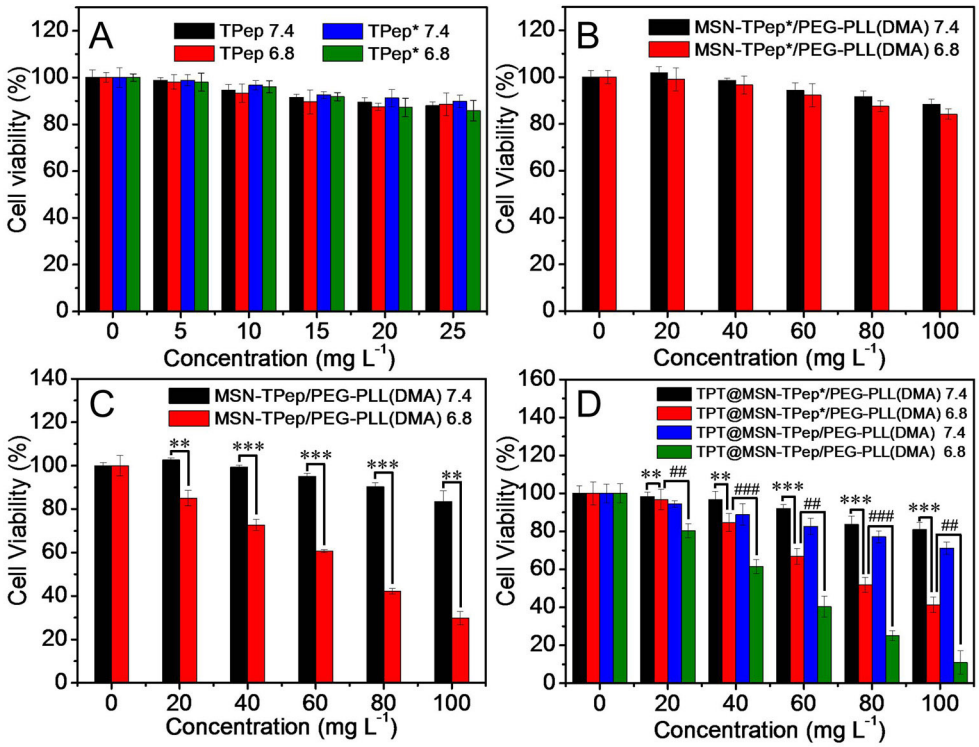

Figure 7 | Cell viability of KB cells incubated with (A) free TPep and TPep*, (B) MSN-TPep*/PEG-PLL(DMA), (C) MSN-TPep/PEG-PLL(DMA), and (D) TPT@MSN-TPep*/PEG-PLL(DMA) and TPT@MSN-TPep/PEG-PLL(DMA) at pH 7.4 and 6.8 (100 mg/L of TPT@MSN-TPep/PEG-PLL(DMA) correspond to ~2.65 mg/L of TPT). Statistical significance in difference was analyzed using student's T-Test: $^{**}p < 0.01$ and $^{***}p < 0.001$; $^{\#\#}p < 0.01$ and $^{\#\#\#}p < 0.001$.

from Shanghai Chemical Reagent Co. and was recrystallized before use. 2-Chlorotrityl chloride resin (100–200 mesh, loading: 1.32 mmol/g), N-fluorenyl-9-methoxycarbonyl (FMOC) protected amino acids (Fmoc-D-Lys(Boc)-OH, Fmoc-D-Ala-OH, Fmoc-D-Leu-OH, Fmoc-Lys(Dde)-OH, and Fmoc-Cys(Trt)-OH), diisopropylethylamine (DiEA), o-benzotriazol-N,N,N′,N′-tetramethyluronium hexafluorophosphate (HBTU), 1-hydroxybenzotriazole (HOBt), piperidine, and triisopropylsilane (TIS) were purchased from GL Biochem Ltd. (Shanghai, China). 2,3-Dimethylmaleic anhydride (DMA) and (3-mercaptopropyl)trimethoxysilane were purchased from Aladdin Reagent Co. Ltd. RPMI-1640 Medium, topotecan hydrochloride, JC-1 (5,5′,6,6′-tetrachloro-1,1′,3,3′-tetraethylbenzimidazolycarbocyanine iodide) fluorescent dye, amino-monomethoxypoly(ethylene glyco) (PEG, Mw 2000), and N(ε)-benzyloxycarebonyl-L-lysine (H-Lys(Z)-OH) were purchased from Sigma-Aldrich. (4-Carboxybutyl) triphenylphosphonium bromide was purchased from Adamas Reagent Co. Ltd. The mitochondria fluorescence probe (Mito Tracker Green FM), penicillin-streptomycin, fetal bovine serum (FBS), 3-(4,5-dimethylthiazol-2-yl)-2,5-diphenyltetrazolium bromide (MTT), and Dulbecco's phosphate buffered saline (PBS) were obtained from Invitrogen. Other reagents and solvents were of analytical grade and were purified before use.

Characterizations. ^{1}H NMR spectra were recorded on a Varian Unity 300 MHz spectrometer by using dimethyl sulfoxide-d_6 (DMSO-d_6) or D_2O as the solvent. The molecular weight and polydispersity index (PDI) of PEG-PLL were evaluated by gel permeation chromatographic (GPC) system consisting of Waters 2690D separations module and Waters 2410 refractive index detector. Tetrahydrofuran (THF) was used as the eluent at a flow rate of 0.3 mL/min. The particle size and zeta potential were measured using Malvern Zetasizer Nano-ZS ZEN3600. Nitrogen adsorption−desorption isotherms were measured on a micromeritics instrument (ASAP2020). Thermal gravitational analysis (TGA) was performed with a Thermo Gravimetric Analyzer (TGS--II, Perkin-Elmer). Fluorescence analysis was performed on a RF-530/PC spectrofluorophotometer (Shimadzu). The morphologies of nanoparticles were observed on scanning electron microscopy (SEM, FEI-QUANTA 200) and transmission electron microscopy (TEM, JEM-2100).

Synthesis of poly(ethylene glycol)-blocked-2,3-dimethylmaleic anhydride-modified poly(L-lysine) (PEG-PLL(DMA)). Brifly, H-Lys(Z)-OH (7.6 g) was dissolved in distilled THF (80 mL) and the mixture was stired at 50°C under N_2 atmosphere. Then a solution of triphosgene (3.4 g) in THF (10 mL) was added dropwise to the suspension and stired for 3 h. The resultant solution was poured into excess n-hexane to obtain Z-Lys-NCA. The crude product was further recrystallixzed from dried THF/n-hexane twice and dried under vacuum. The polymerization of Z-Lys-NCA (1.0 g) by amino-terminated PEG (0.1 g) was carried out in 15 mL anhydrous N,N-dimethylformamide (DMF) at 50°C under N_2 atmosphere for 3 days. The mixture was precipitated in an excess of diethyl ether three times to obtain PEG-PLL(Z). Subsequently, 10 mL TFA was added to dissolve PEG-PLL(Z) (500 mg) in an ice bath. After stirring for 15 min, HBr (5 mL of a 33 wt% solution in acetic acid) was added dropwise and was stirred for another 1 h. Then the solution was precipitated in diethy ether. After collecting and drying, the product was resuspended in 10 mL DMF and the solution was dialyzed (MWCO: 3500 Da) against distilled water for 3 days and finally lyophilized to obtain PEG-PLL. The modification of PEG-PLL (50 mg) with DMA (75 mg, 2 eq. to amino groups) was carried out in a NaOH solution (pH 8) for 24 h under N_2 atmosphere. After completion of the reaction, the excess of DMA was removed by dialyzation against water (the pH value was adjusted to 8.0 by 0.1 M NaOH solution). The final product was obtained by lyophilization.

Synthesis of peptide analogs. All the peptides were synthesized manually with standard solid phase synthesis protocols based on classical Fmoc-chemistry. Briefly, Fmoc-protected amino acid was coupled on a 2-chlorotrityl chloride resin (1.32 mmol/g) in a DMF solution of DiEA/HBTU/HOBt. Fmoc-protecting group was removed with 20% piperidine in DMF (v/v) for twice. Ninhydrin assay was utilized to monitor the coupling efficacy. For synthesis of $(KLAKLAK)_2$ sequence, D-amino acids were used for avoiding proteolysis[62]. (4-Carboxybutyl) triphenylphosphonium bromide and Rhodamine B was coupled using the similar method to amino acid. After the completion of the synthesis, the resin was finally washed with DMF (four times) and dichloromethane (DCM) (four times) and dried under vacuum. Fully removal of side chain protected groups and cleavage of the expected samples from the dried resin were performed by a mixture of TFA/TIS/H_2O (95%/2.5%/2.5%), followed by precipitation in cold ether. The crude product was collected, vacuum dried, resuspended in distilled water and freeze-dried. All the samples listed in Table S1 were synthesized and the purity was examined by high-pressure liquid chromatography (HPLC) with a C_{18} column using a liner gradient of acetonitrile and deionized water containing 0.1% TFA.

Synthesis of silica nanoparticles. Briefly, CTAB (1.0 g, 2.74 mmol) and NaOH (0.28 g, 7 mmol) were first dissolved in 480 mL of deionized water and the solution was stirred at 80°C for 15 min. Then, 5.36 mL TEOS was added dropwise to the suspension under vigorous stirring. After stirring for another 2 h at 80°C, the resulting white precipitate was centrifuged, washed thoroughly with deionized water and methanol, and dried under vacuum.

Surface modification of mesoporous silica nanoparticles. The above obtained silica nanoparticles (500 mg) were first modified with (3-

mercaptopropyl)trimethoxysilane (5 mL) in 30 mL methanol upon stirring at room temperature overnight. CTAB was removed by refluxing the nanoparticles (500 mg) in a mixture of methanol (100 mL) and 37.4% HCl (6 mL) for 24 h at 60°C to obtain mesoporous MSN-SH. Then, MSN-SH particles (300 mg) were dispersed in 30 mL methanol solution containing 2,2′-dipyridyl disulfide (100 mg). The solution was further stirred at room temperature overnight. Subsequently, 50 mg of the above resulting material and TPep (50 mg) were dispersed in 30 mL DMF and stirred at room temperature for 24 h to obtain the desired MSN-TPep. 50 mg of MSN-TPep was finally dispersed in 10 mL of phosphate buffer solution (PBS) (10 mM, pH 8.0), followed by adding PEG-PLL(DMA) (6 mg) and stirring for 4 h to obtain MSN-TPep/PEG-PLL(DMA). After each functionalization step, the particles were isolated by centrifugation, washed with methanol or PBS (10 mM, pH 8.0), and dried under vacuum. MSN-TPep*/PEG-PLL(DMA), MSN-TPep(Rh B)/PEG-PLL(DMA), and MSN-Pep/PEG-PLL(DMA) were prepared according to a similar procedure.

Surface charge conversion of nanoparticles at different pHs. MSN-TPep/PEG-PLL(DMA) nanoparticles were incubated in 10 mM PBS at a pH of 7.4 or 6.8 with a concentration of 1 mg/mL at 37°C, respectively. At designated time intervals, the zeta-potentials were measured by Malvern Zetasizer Nano-ZS ZEN3600.

Topotecan (TPT) loading. 100 mg of MSN-SH were suspended in 15 mL of topotecan hydrochloride solution (1 mg/mL) in PBS (10 mM, pH 7.4) and stirred at room temperature overnight. The nanoparticles were isolated by centrifugation and carefully washed with PBS three times. The programmed packing of TPT-loaded MSN-SH with TPep and PEG-PLL(DMA) were similar to the procedure described above. The resulting TPT@MSN-TPep/PEG-PLL(DMA) nanoparticles were collected. The drug loading content was determined by fluorescence analysis. After completely dissolving of 1 mg TPT@MSN-TPep/PEG-PLL(DMA) in 0.1 M HF solution, the pH value of the dissolution was adjusted to ~7.4 with 0.1 M NaOH solution. The dissolution was subsequently analyzed by RF-5301PC spectrofluorophotometer.

***In vitro* release study.** *In vitro* release experiments were carried out in four different media: PBS without GSH at pH 7.4, PBS with 10 mM GSH at pH 7.4, PBS without GSH at pH 6.8, and PBS with 10 mM GSH at pH 6.8, respectively. For each release study, 5 mg of the corresponding nanoparticles (MSN-Tpep(Rh B)/PEG-PLL(DMA) for Tpep(Rh B) release study and TPT@MSN-Tpep/PEG-PLL(DMA) for TPT release study) were suspended in 2 mL PBS buffer solution. The solution was put into a dialysis tube (MWCO: 12 kDa) which was directly immersed into 10 mL incubation medium and maintained at 37°C. After particular time intervals, fluorescence intensity of the incubation medium was analyzed by RF-5301PC spectrofluorophotometer (λex = 488 nm for TPep(Rh B), λex = 350 nm for TPT). The cumulative release of TPT or TPep(Rh B) was calculated according to the respective standard curve.

Confocal laser scanning microscopy. KB cells (human mouth epidermal carcinoma cells) were seeded in a glass bottom dish in RPMI-1640 medium (1 mL) with 10% FBS and 1% antibiotics (penicillin-streptomycin, 10,000 U/mL) and incubated in a humidified atmosphere containing 5% CO_2 at 37°C for 24 h. For cell uptake evaluation, free TPep(Rh B) (5 mg/L), and MSN-TPep(Rh B)/PEG-PLL(DMA) (50 mg/L) dispersed in RPMI-1640 medium (1 mL) were added and the cells were further incubated at 37°C for another 4 h. Subsequently, the mitochondria were stained with 100 nM Mito Tracker Green FM in RPMI-1640 medium (without FBS) for 30 min. After removing the medium and washing with PBS, the cells were observed under a confocal microscopy (CLSM, Nikon C1-si TE2000, BD Laser). For cell uptake of TPT@MSN-TPep(Rh B)/PEG-PLL(DMA), 1 mL of RPMI-1640 medium containing nanoparticles (30 mg/L) was added and the cells were incubatied for 4 h at 37°C. After removing the medium and washing with PBS, the cells were observed under a confocal microscopy. For JC-1 assay, MSN-TPep/PEG-PLL(DMA) (50 mg/L) dispersed in RPMI-1640 medium (1 mL) were added and the cells were further incubated at 37°C for 12 h or 36 h. The mitochondria were stained with JC-1 (10 μg/mL) in RPMI-1640 medium for another 30 min. After removing the medium and washing with PBS, the cells were observed under a confocal microscopy.

Flow cytometry analysis. KB cells were seeded in 6-well plates (5×10^4 cells/well) and cultured in RPMI-1640 medium (1 mL) containing 10% FBS and 1% antibiotics for 24 h. After that, free TPep(Rh B) (5 mg/L) and MSN-TPep(Rh B)/PEG-PLL(DMA) (50 mg/L) dispersed in DMEM medium (1 mL) were added and the cells were further incubated at 37°C for another 4 h. Then the medium was removed and the cells were washed three times with PBS. All the cells were digested by trypsin, collected in centrifuge tubes, and washed twice with PBS (pH 7.4). The suspended cells were filtrated and examined by flow cytometry (BD FACSAria™ III). Cells without treatment were used as control.

Bio-TEM observation. For TEM observation, after co-incubation of KB cells with nanoparticles, the cells were washed with PBS for 3 times to remove excess nanoparticles and fixed with 1 mL general fixative (containing 2.5% glutaraldehyde in 0.1 M PBS) at 4°C overnight. Subsequently, the cells were collected, embedded in epoxy resin and sliced with a thickness of 50–70 nm. Finally, the cell section was stained with 5% uranyl acetate and 2% lead citrate for 15 min for observation.

***In vitro* cytotoxicity.** KB cells were seeded in a 96-well plate (1.5×10^4 cells/well) containing RPMI-1640 media (200 μL), followed by incubation for one day (37°C, 5% CO_2). Then, the culture media was replaced with 200 μL medium containing particular materials (free TPep*, free TPep, MSN-TPep*/PEG-PLL(DMA), MSN-TPep/PEG-PLL(DMA), TPT@MSN-TPep*/PEG-PLL(DMA), and TPT@MSN-TPep/PEG-PLL(DMA)) at different doses. The pH of the incubation medium in some wells was adjusted to 6.8 with 1 M HCl. After co-incubated for two days, the medium was replaced with 200 μL of fresh medium. Then, 20 μL of MTT solution (5 mg/mL) was added to each well and the cells were further incubated for 4 h. Subsequently, the medium was removed and DMSO (200 μL) was added. The optical density (OD) was measured at 570 nm with a microplate reader (BIO-RAD 550). The relative cell viability was calculated as: cell viability (%) = $(OD_{treated}/OD_{control}) \times 100\%$. Each value was averaged from four independent experiments.

1. Ghosh, P., Han, G., De, M., Kim, C. K. & Rotello, V. M. Gold nanoparticles in delivery applications. *Adv. Drug Deliv. Rev.* **60**, 1307–13015 (2008).
2. Xiong, H. M. ZnO nanoparticles applied to bioimaging and drug delivery. *Adv. Mater.* **25**, 5329.–5335 (2013).
3. Jain, T. K. *et al.* Magnetic nanoparticles with dual functional properties: drug delivery and magnetic resonance imaging. *Biomaterial* **29**, 4012–4021 (2008).
4. Shin, J. *et al.* Hollow manganese oxide nanoparticles as multifunctional agents for magnetic resonance imaging and drug delivery. *Angew. Chem. Int. Ed.* **48**, 321–324 (2009).
5. Quan, C. Y. *et al.* Core-shell nanosized assemblies mediated by the α-β cyclodextrin dimer with a tumor-triggered targeting property. *ACS Nano* **4**, 4211–4219 (2010).
6. Al-Ahmady, Z. S. *et al.* Lipid-peptide vesicle nanoscale hybrids for triggered drug release by mild hyperthermia in vitro and in vivo. *ACS Nano* **6**, 9335–9346 (2012).
7. Nakamura, T., Akita, H., Yamada, Y., Hatakeyama, H. & Harashima, H. A multifunctional envelope-type nanodevice for use in nanomedicine: concept and applications. *Acc. Chem. Res.* **45**, 1113–1121 (2012).
8. Zhang, E., Zhang, C., Su, Y., Cheng, T. & Shi, C. Newly developed strategies for multifunctional mitochondria-targeted agents in cancer therapy. *Drug Discov. Today* **16**, 140–146 (2011).
9. Knop, K., Hoogenboom, R., Fischer, D. & Schubert, U. S. Poly(ethylene glycol) in drug delivery: pros and cons as well as potential alternatives. *Angew. Chem. Int. Ed.* **49**, 6288–6308 (2010).
10. Otsuka, H., Nagasaki, Y. & Kataoka, K. PEGylated nanoparticles for biological and pharmaceutical applications. *Adv. Drug Deliv. Rev.* **64**, 246–255 (2012).
11. Yang, X. Z. *et al.* Sheddable ternary nanoparticles for tumor acidity-targeted siRNA delivery. *ACS Nano* **6**, 771–781 (2012).
12. Mok, H., Park, J. W. & Park, T. G. Enhanced intracellular delivery of quantum dot and adenovirus nanoparticles triggered by acidic pH via surface charge reversal. *Bioconjug. Chem.* **19**, 797–801 (2008).
13. Yang, X. Z. *et al.* Sheddable ternary nanoparticles for tumor acidity-targeted siRNA delivery. *ACS Nano* **6**, 771–781 (2012).
14. van der Aa, M. A. E. M. *et al.* The unclear pore complex: the gateway to successful nonviral gene delivery. *Pharm. Res.* **23**, 447–459 (2006).
15. Mizutani, H., Tada-Oikawa, S., Hiraku, Y., Kojima, M. & Kawanishi, S. Mechanism of apoptosis induced by doxorubicin through the generation of hydrogen peroxide. *Life Sci.* **76**, 1439–1451 (2005).
16. Pavillard, V., Kherfellah, D., Richard, S., Robert, J. & Montaudon, D. Effects of the combination of camptothecin and doxorubicin or etoposide on rat glioma cells and camptothecin-resistant variants. *Br. J. Cancer* **85**, 1077–1083 (2001).
17. Wang, H., Wu, Y., Zhao, R. & Nie, G. Engineering the assemblies of biomaterial nanocarriers for delivery of multiple theranostic agents with enhanced antitumor efficacy. *Adv. Mater.* **25**, 1616–1622 (2013).
18. Fan, H. *et al.* In vivo treatment of tumors using host-guest conjugated nanoparticles functionalized with doxorubicin and therapeutic gene pTRAIL. *Biomaterials* **33**, 1428–1436 (2012).
19. Wang, Y., Gao, S., Ye, W. H., Yoon, H. S. & Yang, Y. Y. Co-delivery of drugs and DNA from cationic core–shell nanoparticles self-assembled from a biodegradable copolymer. *Nat. Mater.* **5**, 791–796 (2006).
20. Meng, H. *et al.* Codelivery of an optimal drug/siRNA combination using mesoporous silica nanoparticles to overcome drug resistance in breast cancer in vitro and in vivo. *ACS Nano* **7**, 994–1005 (2013).
21. Shen, Y. Q. *et al.* Prodrugs forming high drug loading multifunctional nanocapsules for intracellular cancer drug delivery. *J. Am. Chem. Soc.* **132**, 4259–4265 (2010).
22. Verma, M., Kagan, J., Sidransky, D. & Srivastava, S. Proteomic analysis of cancer-cell mitochondria. *Mat. Rev. Cancer* **3**,789–795 (2013).
23. He, Q. & Shi, J. MSN anti-cancer nanomedicines: chemotherapy enhancement, overcoming of drug resistance, and metastasis inhibition. *Adv. Mater.* **26**, 391–411 (2013).
24. Tarn, D. *et al.* Mesoporous silica nanoparticle nanocarriers: biofunctionality and biocompatibility. *Acc. Chem. Res.* **46**, 792–801 (2014).
25. Lai, J., Shah, B. P., Garfunkel, E. & Lee, K. B. Versatile fluorescence resonance energy transfer-based mesoporous silica nanoparticles for real-time monitoring of drug release. *ACS Nano* **7**, 2741–2750 (2013).

26. Pan, L., Liu, J., He, Q., Wang, L. & Shi, J. Overcoming multidrug resistance of cancer cells by direct intranuclear drug delivery using TAT-conjugated mesoporous silica nanoparticles. *Biomaterials* **34**, 2719–2730 (2013).
27. Xing, L., Zheng, H., Cao, Y. & Che, S. Coordination polymer coated mesoporous silica nanoparticles for pH-responsive drug release. *Adv. Mater.* **24**, 6433–6437 (2012).
28. He, Q., Shi, J., Chen, F., Zhu, M. & Zhang, L. An anticancer drug delivery system based on surfactant-templated mesoporous silica nanoparticles. *Biomaterials* **31**, 3335–3346 (2010).
29. Lu, J., Liong, M., Zink, J. I. & Tamanoi, F. Mesoporous silica nanoparticles as a delivery system for hydrophobic anticancer drugs. *Small* **3**, 1341–1346 (2007).
30. Zhang, Z. *et al.* Biocatalytic release of an anticancer drug from nucleic-acids-capped mesoporous SiO_2 using DNA or molecular biomarkers as triggering stimuli. *ACS Nano* **7**, 8455–8468 (2013).
31. Dong, J., Xue, M. & Zink, J. I. Functioning of nanovalves on polymer coated mesoporous silica nanoparticles. *Nanoscale* **5**, 10300–10306 (2013).
32. Luo, Z. *et al.* Engineering a hollow nanocontainer platform with multifunctional molecular machines for tumor-targeted therapy in vitro and in vivo. *ACS Nano* **7**, 10271–10284 (2013).
33. Kim, H. *et al.* Glutathione-induced intracellular release of guests from mesoporous silica nanocontainers with cyclodextrin gatekeepers. *Adv. Mater.* **22**, 4280–4283 (2010).
34. Zhao, Y. L. *et al.* pH-operated nanopistons on the surfaces of mesoporous silica nanoparticles. *J. Am. Chem. Soc.* **132**, 13016–13025 (2010).
35. Angelos, S., Yang, Y. W., Patel, K., Stoddart, J. F. & Zink, J. I. pH-responsive supramolecular nanovalves based on cucurbit[6]uril pseudorotaxanes. *Angew. Chem. Int. Ed.* **47**, 2222–2226 (2008).
36. Thomas, C. R. *et al.* Noninvasive remote-controlled release of drug molecules in vitro using magnetic actuation of mechanized nanoparticles. *J. Am. Chem. Soc.* **132**, 10623–10625 (2010).
37. Zhu, C. L. *et al.* An efficient cell-targeting and intracellular controlled-release drug delivery system based on MSN-PEM-aptamer conjugates. *J. Mater. Chem.* **19**, 7765–7770 (2009).
38. Radu, D. R. *et al.* A polyamidoamine dendrimer-capped mesoporous silica nanosphere-based gene transfection reagent. *J. Am. Chem. Soc.* **126**, 13216–13217 (2004).
39. Chen, A. M. *et al.* Co-delivery of doxorubicin and Bcl-2 siRNA by mesoporous silica nanoparticles enhances the efficacy of chemotherapy in multidrug-resistant cancer cells. *Small* **5**, 2673–2677 (2009).
40. Chen, C. *et al.* Polyvalent nucleic acid/mesoporous silica nanoparticle conjugates: dual stimuli-responsive vehicles for intracellular drug delivery. *Angew. Chem. Int. Ed.* **50**, 882–886 (2011).
41. Schlossbauer, A., Kecht, J. & Bein, T. Biotin–avidin as a protease-responsive cap system for controlled guest release from colloidal mesoporous silica. *Angew. Chem. Int. Ed.* **48**, 3092–3095 (2009).
42. Zhu, C. L., Lu, C. H., Song, X. Y., Yang, H. H. & Wang, X. R. Bioresponsive controlled release using mesoporous silica nanoparticles capped with aptamer-based molecular gate. *J. Am. Chem. Soc.* **133**, 1278–1281 (2011).
43. Giri, S., Trewyn, B. G., Stellmaker, M. P. & Lin, V. S. Y. Stimuli-responsive controlled-release delivery system based on mesoporous silica nanorods capped with magnetic nanoparticles. *Angew. Chem. Int. Ed.* **44**, 5038–5044 (2005).
44. Muhammad, F. *et al.* pH-triggered controlled drug release from mesoporous silica nanoparticles via intracelluar dissolution of ZnO nanolids. *J. Am. Chem. Soc.* **133**, 8778–8781 (2011).
45. Lai, C. Y. *et al.* A mesoporous silica nanosphere-based carrier system with chemically removable CdS nanoparticle caps for stimuli-responsive controlled release of neurotransmitters and drug molecules. *J. Am. Chem. Soc.* **125**, 4451–4459 (2003).
46. Li, Z. Y. *et al.* One-pot construction of functional mesoporous silica nanoparticles for the tumor-acidity-activated synergistic chemotherapy of glioblastoma. *ACS Appl. Mater. Interfaces* **5**, 7995–8001 (2013).
47. Fugit, K. D. & Anderson, B. D. The role of pH and ring-opening hydrolysis kinetics on liposomal release of topotecan. *J. Control Release* **174**, 88–97 (2014).
48. Marrache, S. & Dhar, S. Engineering of blended nanoparticle platform for delivery of mitochondria-acting therapeutics. *Proc. Natl. Acad. Sci. U.S.A.* **109**, 16288–16293 (2012).
49. Agemy, L. *et al.* Targeted nanoparticle enhanced proapoptotic peptide as potential therapy for glioblastoma. *Proc. Natl. Acad. Sci. U.S.A.* **108**, 17450–17455 (2011).
50. Du, J. Z., Sun, T. M., Song, W. J., Wu, J. & Wang, J. A tumor-acidity-activated charge-conversional nanogel as an intelligent vehicle for promoted tumoral-cell uptake and drug delivery. *Angew. Chem. Int. Ed.* **49**, 3621–3626 (2010).
51. Yuan, Y. Y. *et al.* Surface charge switchable nanoparticles based on zwitterionic polymer for enhanced drug delivery to tumor. *Adv. Mater.* **24**, 5476–5480 (2012).
52. Fields, G. B. & Noble, R. L. Solid phase peptide synthesis utilizing 9-fluorenylmethoxycarbonyl amino acids. *Int. J. Pept. Protein Res.* **35**, 161–214 (1990).
53. Leung, C. W. *et al.* A photostable AIE luminogen for specific mitochondrial imaging and tracking. *J. Am. Chem. Soc.* **135**, 62–65 (2013).
54. Wang, X. H. *et al.* Poly-L-lysine assisted synthesis of core–shell nanoparticles and conjugation with triphenylphosphonium to target mitochondria. *J. Mater. Chem. B* **1**, 5143–5152 (2013).
55. Fleige, E., Quadir, M. A. & Haag, R. Stimuli-responsive polymeric nanocarriers for the controlled transport of active compounds: concepts and applications. *Adv. Drug Deliv. Rev.* **64**, 866–884 (2012).
56. Dhar, S. & Lippard, S. J. Mitaplatin, a potent fusion of cisplatin and the orphan drug dichloroacetate. *Proc. Natl. Acad. Sci. U.S.A.* **106**, 22199–22204 (2009).
57. Hong, R. *et al.* Glutathione-mediated delivery and release using monolayer protected nanoparticle carriers. *J. Am. Chem. Soc.* **128**, 1078–1079 (2006).
58. Asefa, T. & Tao, Z. Biocompatibility of mesoporous silica nanoparticles. *Chem. Res. Toxicol.* **25**, 2265–2284 (2012).
59. Chen, Y., Chen, H. & Shi, J. In vivo bio-safety evaluations and diagnostic/therapeutic application of chemically designed mesoporous silica nanoparticles. *Adv. Mater.* **25**, 3314–3376 (2013).
60. Lu, J., Liong, M., Li, Z., Zink, J. I. & Tamanoi, F. Biocompatibility, biodistribution, and drug-delivery efficiency of mesoporous silica nanoparticles for cancer therapy in animals. *Small* **6**, 1794–1805 (2010).
61. Souris, J. S. *et al.* Surface charge-meditated rapid hepatobiliary excretion of mesoporous silica nanoparticles. *Biomaterials* **31**, 5564–5574 (2010).
62. Bessalle, R., Kapitkovsky, A., Gorea, A., Shalit, I. & Fridkin, M. All-D-magainin: chirality, antimicrobial activity and proteolytic resistance. *FEBS Lett.* **274**, 151–155 (1990).

Acknowledgments

This work was financially supported by the National Natural Science Foundation of China (51125014, 51233003), National Key Basic Research Program of China (2011CB606202), the Ministry of Education of China (20120141130003) and supported by the Fundamental Research Funds for the Central Universities (2014203020201 and 2014203020204).

Author contributions

G.F.L. and Z.X.Z. conceived and designed the experiments. G.F.L., W.H.C., Y.L. and Q.L. performed the experiments. G.F.L., R.X.Z. and Z.X.Z. analyzed the data and co-wrote the paper.

Additional information

Supplementary information accompanies this paper at http://www.nature.com/scientificreports

Competing financial interests: The authors declare no competing financial interests.

How to cite this article: Luo, G.-F. *et al.* Multifunctional Enveloped Mesoporous Silica Nanoparticles for Subcellular Co-delivery of Drug and Therapeutic Peptide. *Sci. Rep.* **4**, 6064; DOI:10.1038/srep06064 (2014).